ACS Photonics

Article

pubs.acs.org/journal/apchd5

Parametric Force Analysis for Measurement of Arbitrary Optical Forces on Particles Trapped in Air or Vacuum

Haesung Park and Thomas W. LeBrun*

Physical Measurement Laboratory, National Institute of Standards and Technology, Gaithersburg, Maryland 20899, United States

ABSTRACT: We demonstrate a new method to measure arbitrary optical forces on particles trapped in gaseous or vacuum environments using the ring down of a trapped particle following electrostatic excitation of particle motion in the trap. The method is not limited to the common constraints of linear forces for small oscillations or conservative forces, allows for a wide displacement range, and measures forces directly from trajectories in near-real time. We use transient response analysis to model the nearly ideal response for small oscillations, and illustrate the more general case by demonstrating a nonlinear response to impulse excitation at a displacement where the optical force is linear. Simulations verify the applicability to nonlinear forces from a general potential, and comparison to traditional thermodynamic measures shows good agreement. Combined with in situ microscopy to measure the particle diameter, this allows for the estimation of all system parameters assuming only the manufacturer's value for the particle density.

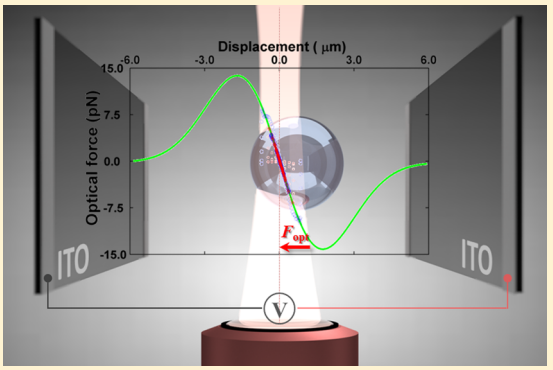

KEYWORDS: *optical trapping, optical levitation, optical force measurement, transient response analysis, parametric force analysis*

Optical tweezers have been studied extensively for precise manipulation and measurement[1,2] of samples ranging from micro- and nanoscale particles[3] to biomolecules[4] and single atoms.[5] Force measurement is central to many of the precision measurements performed with optical tweezers, and a number of force and displacement measurement techniques have been developed for trapping in fluid media.[4,6−8] More recently, trapping particles in air or vacuum has experienced a resurgence of interest, in part because of the high environmental isolation attained by trapping in vacuum, which can provide a route to the long coherence times required to prepare and manipulate microscopic objects in quantum states.[9−11] However, the force measurement methods developed for particles in liquids may not be directly applicable to gas-phase trapping because forces ignored in liquids, such as particle inertia, play significant roles in gas-phase trapping.[12,13] In addition, the significantly reduced damping can lead to oscillations and potential instability that complicate measurement,[14] and the generic assumption of thermal equilibrium (or assumed values of temperature and viscosity) based on the superior thermal conductivity of liquids may not be applicable.[15]

To date, force measurements in gas or vacuum typically rely on statistical approaches that measure over a limited range of thermal fluctuations (a few tens of nanometers) to estimate the force near center without determining the range of validity of the linear approximation. This also does not capture the variability in the thermal conditions of the particle and medium[16] or the importance of simultaneous measurement of trapping stiffness and calibration of position detection sensitivity in situ, an important consideration in maintaining accurate calibrations that match the specific particle in the trap.[17−19]

We use the ring down of a trapped particle in air following electrostatic excitation combined with video microscopy for particle size measurement to completely determine the system parameters. This allows particle mass, charge, diameter, and the full optical force in one dimension to be determined without assuming small oscillations, linearity, or the value of the viscous damping coefficient of the medium. We assume only the manufacturer's value of the particle density. Temperature is also estimated by noting that the damping is not consistent with air at 20 °C, and calculating the temperature required to give an air viscosity that yields the measured damping.[20]

In the following we combine photodiode-based particle tracking measurements with video microscopy, first measuring the transient response to a step change in the electrostatic field. This determines the damping and trap stiffness for small oscillations and allows the quadrant-cell photodetector (QPD) response to be calibrated directly from the experimental data for each particle measured. A simple transformation of the particle trajectory yields the optical force curve in parametric form with no restriction to small oscillations. This allows a simple and direct measurement of the optical forces effectively in real time and over a range of displacement that far exceeds both the thermal trapping volume and the range of linear response. This could enable a range of studies from the nonlinear dynamics of particle motion at high excitation to precision 3D measurements of optical fields and forces. A comparison of the measured values to each other and to known thermodynamic relations shows good

Received: June 2, 2015
Published: September 8, 2015

DOI: 10.1021/acsphotonics.5b00309
ACS Photonics 2015, 2, 1451−1459

agreement and allows temperature to be estimated separately from external factors such as vibration or measurement noise.

RESULTS AND DISCUSSION

The instrument uses an inverted microscope to produce a vertically directed laser beam that traps particles within a small rectangular glass cell. A voltage applied to two opposite (conductive) sides of the cell excites particle motion in the trap. The motion is tracked using both light scattered onto a quadrant photodiode and video microscopy. Figure 1 illustrates the

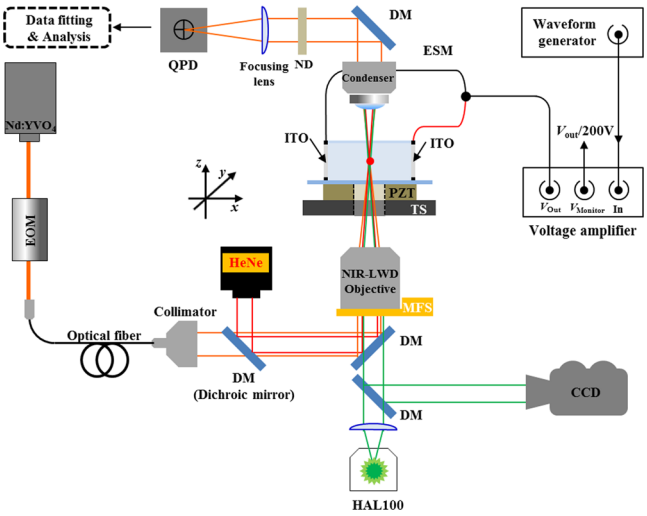

Figure 1. Schematic drawing of the optical tweezers setup used in this study. EOM, electro-optic modulator; HAL100, halogen illuminator; MFS, motorized focusing stage; NIR-LWD objective, infrared corrected long working distance objective lens; TS, translation stage (x, y); PZT, piezoelectric transducer; ESM, electrostatic field modulator; ND, neutral density filter; QPD, quadrant-cell photodetector. Imaging is also performed along the y-axis direction perpendicular to the applied electric field (not shown). The instrument uses a commercial inverted optical microscope (Eclipse TE2000).

approach. A fiber-coupled laser is loosely focused with a long-working distance objective lens onto the glass substrate. To launch the particle, a piezoelectric transducer momentarily breaks the adhesion of the polystyrene (PS) particle to the glass substrate[21] so that radiation pressure controllably lifts the particle (diameter = 22.12 μm) into the trapping volume. The motion of the particle (which is charged due to contact electrification) is excited by an electrostatic field generated from two parallel plates (indium tin oxide (ITO) coated coverslips) attached to the sample enclosure, as shown in Figure 2 (a). Because of the large gain of the voltage amplifier and charge on the particle (approximately 3990 electrons for the measurement reported here), the particle can be freely moved over a few micrometers while we measure the particle position through video microscopy and a position-sensitive detector (see Figure 2 (b) and (c)). The details of the experimental setup and procedure including sample preparation, loading, enclosure, particle size measurement, and calibration of position detector are described in the Methods section.

The motion of a trapped particle (including Brownian motion) can be described by the Langevin equation,[22]

$$m\ddot{\mathbf{r}} + \gamma\dot{\mathbf{r}} - \mathbf{F}_{\mathbf{opt}}(r, t) = m\mathbf{A}_{\mathbf{rand}}(t) \quad (1)$$

where $\mathbf{r}$ is the particle position, m the mass, γ the coefficient of friction (calculated here using Stokes law: $\gamma = 6\pi R\eta$ where

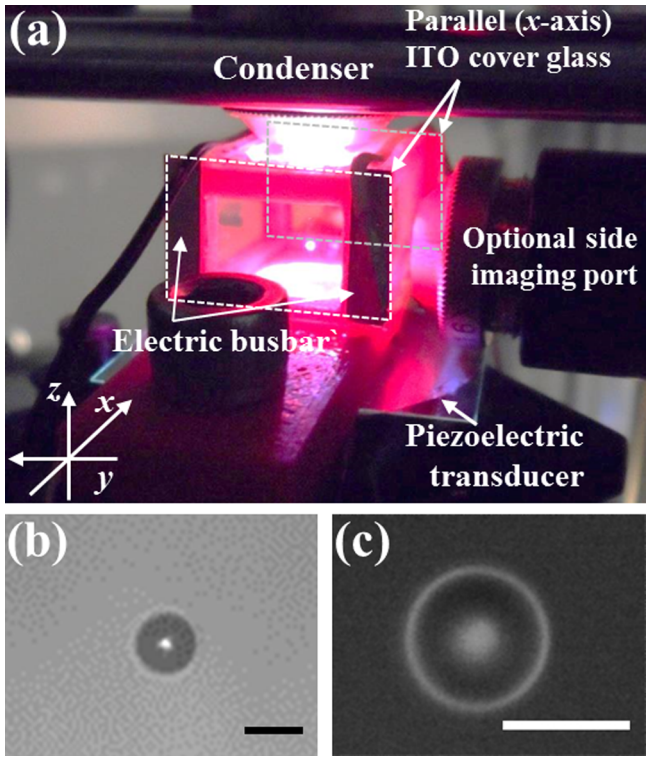

Figure 2. (a) Levitation cell showing a trapped particle through one of the two parallel ITO coated cover glasses used in the sample enclosure to enable electrostatic field modulation. (b) A trapped particle observed through the optional side imaging port and (c) imaged through the NIR corrected LWD objective lens (both scale bars indicate 20 μm). The particle motion under electrostatic field modulation can be measured using both CCDs and the QPD simultaneously.

R and η denote the particle radius and dynamic viscosity of surrounding medium), $\mathbf{F}_{\mathbf{opt}}$ the optical force, and $m\mathbf{A}_{\mathbf{rand}}$ the Langevin force. Boldface represents vector quantities. For small (linear) oscillations in one dimension eq 1 becomes

$$\ddot{x} + \beta\dot{x} + \omega_0^2 x = A(t) \quad (2)$$

with β^{-1} the relaxation time for the particle energy, $(\beta/2)^{-1}$ the relaxation time for the amplitude of motion through damping ($\beta = \gamma/m$), and $Q = \omega_0/\beta$, where $Q = 0.5$ corresponds to critical damping ($\beta_{\text{critical}} = 2\omega_0$). The random acceleration A and friction are related via the fluctuation−dissipation theorem,[23] with the probability density function for the random acceleration A integrated over a time Δt given by a Gaussian distribution $(4\pi\xi\Delta t)^{-3/2}$ $\exp(-|\mathbf{A}(\Delta t)|^2/4\xi\Delta t)$ where $\xi = \beta k_B T/m$ with Boltzmann constant k_B. For more information see the elegant exposition by Chandrasekar.[22]

For heavily damped systems, Brownian motion dominates the particle motion and statistics of the trajectories are typically used to determine properties of the system.[24] For the underdamped systems studied here the motion is ballistic and simply described using classical mechanics. We average several trajectories for one particle measured under identical conditions to determine the mean trajectory corresponding to a solution of eq 2 with no random forcing term (i.e., $x'' + \beta x' + \omega_0^2 x = 0$). If a constant external force is suddenly applied that is small compared to the maximum trapping force, the particle will jump to a new position, resulting in damped oscillations about the new position (i.e., ring down). Measurement of this motion (the transient response, TR) allows the determination of ω_0 and β.[17,25] To simplify the

DOI: 10.1021/acsphotonics.5b00309
ACS Photonics 2015, 2, 1451−1459

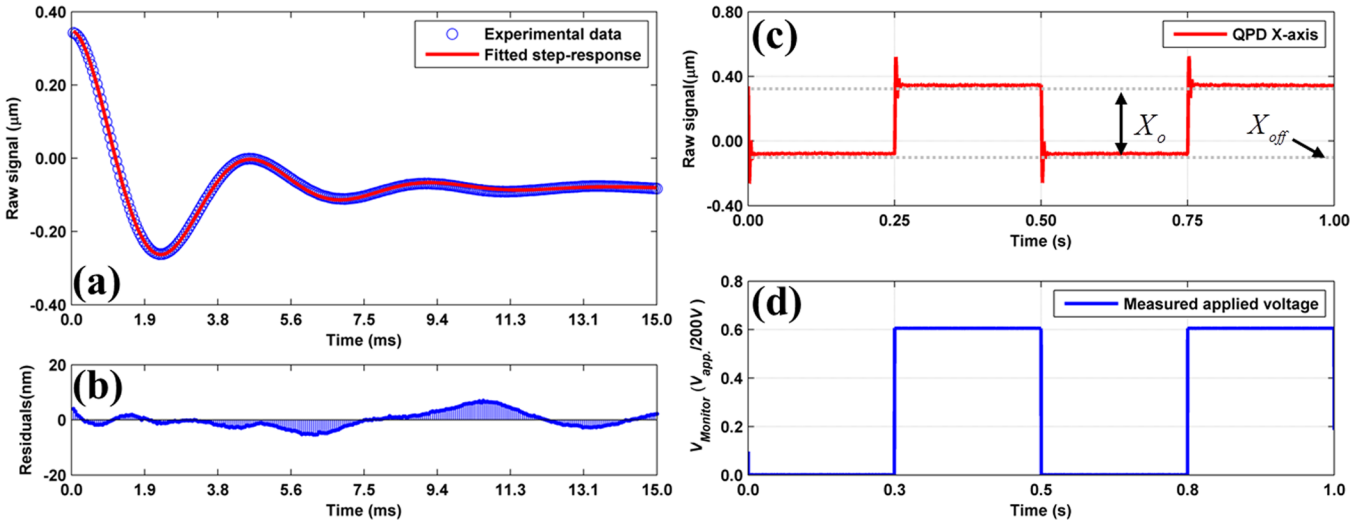

Figure 3. Excitation and response of the trapped 22.12 μm PS bead is measured using the QPD and averaged over 50 cycles of square wave electrostatic modulation with frequency fmod of 2 Hz and 50% duty cycle over 0 to 120 V. (a) Transient step-response of trapped particle fitted to eq 3 with (b) fitting residuals, during 15 ms of (c) repeated step response and (d) measured square wave driving voltage. The trapping laser power is fixed at 125 mW and measured at the back aperture of the objective lens. From the fitting of particle trajectories in displacement, we are able to extract stead steady-state displacement (X_0), QPD offset (X_{off}), natural resonant frequency (ω_0), damping ratio (ζ), and additional phase shift (Φ_{add}).

Table 1. Results Obtained from Nonlinear Least Square Fit of the Experimental Trajectories Displayed in Figure 3 to the eq 3

	transient response measurements[a]						
fitting coefficients [units]	X_0 [μm]	X_{off} [μm]	$\omega_0/2\pi$ [1/s]	β (= $2\varsigma\omega_0$) [1/s]	Q (= $1/2\varsigma$) [pure]	k (= $m\omega_0^2$)[b] [μN/m]	q (e^-)[d] [electrons]
values	−0.4276	0.3468	225.7	743.9	1.91	11.97	3994
(95% CB[c])	±0.0017	±0.0017	±0.5	±6.3	±0.02		

[a]These values are directly extracted from the fitting of particle trajectories in displacements. [b]The stiffness was calculated ($m = \rho_{PS}4/3\pi R^3$) based on the particle diameter ($2R$) measured by video microscopy, while the materials density (ρ_{PS}) is provided by manufacturer. [c]CB: confidence bound [d]The net charge is estimated using the optical restoring force ($F = X_0k$) balanced with Coulomb force ($F = qE$) under uniform electric field ($E = V/d$) generated from two ITO surfaces separated over known distance (d = 15 mm).

transient response formula we define the damping ratio to be $\varsigma = \beta/\beta_{critical}$ (= $\beta/2\omega_0 = 1/2Q$). Assuming a step-change in the electrostatic field, the response can be represented by

$$x(t) = X_0\left(1 - \frac{e^{-\varsigma\omega_0 t}}{\sqrt{1-\varsigma^2}}\sin(\omega_0\sqrt{1-\varsigma^2}\,t + \varphi_d + \Phi_{add})\right) + X_{off} \quad (3)$$

where $x(t)$ is the time-dependent particle displacement from trapping center, X_0 the particle displacement for a DC voltage equal to the step height, X_{off} the initial QPD center offset, and $\phi_d = \tan^{-1}((1-\varsigma^2)^{1/2}/\varsigma)$.[26] In order to account for the arbitrary phase of the step excitation we introduced an additional phase shift term (Φ_{add}). After the transient response, the particle settles down to a steady-state (constant) displacement $X_0(= -qkV/d)$, where k is the stiffness, q the charge, V the voltage and d the distance between the ITO-coated coverslips. Measuring X_0, therefore allows us to determine the charge once k is known. Comparing X_0 to the displacement measured using microscopy (described in the Methods section) allows the QPD to be calibrated over a wide range of motion for each particle used.[17]

To analyze the transient response, the particle trajectories are truncated after the settling time (τ_s) required to relax to within 2% of the steady state value ($\tau_s = -\ln 0.02/\beta$ or 12.3 ms in the case of Figure 3 and Table 1). After this settling time, the measured transient response becomes small and dominated by Brownian motion, as shown in Figure 3 (c). Therefore, all the trajectory signals used in this work are averaged over 50 runs for a period of 15 ms. Although the fluctuations could represent electronic noise or vibrations, we show later that thermal motion dominates the observed fluctuations.

Figure 3 (a) shows the averaged trajectory (blue circles) over 15 ms (from 0.5 to 0.515 s of Figure 3 (c)) and the fit to eq 3 (red curve) with residuals (Figure 3 (b)). Averaging 50 trajectories reduces the contribution of Brownian motion to TR measurements and shows the nearly ideal form of the temporal response, with fit residuals of a few percent. The excitation conditions used here ensure that ring down dominates the early part of the trajectory for TR analysis, while thermally driven Brownian motion dominates the latter part. This allows the same measured trajectories to be used to compare TR and statistical analysis under identical conditions. Figures 3 (c) and (d) show the measured trajectory of the same particle and the voltage monitor of the high voltage amplifier over two periods of step excitation (1 s). The voltage amplifier provides a nearly ideal step-like signal with negligible slew-rate limitation within our experimental sampling rate of 20 kHz. Because of the relatively low resonant frequency of our 20 μm bead (f_0 < 300 Hz), the transient response is easily measured without significant error from the time response or delay of the measurement electronics (QPD, waveform generator, and power amplifier) which have temporal responses in the microsecond range—significantly faster than the experimental time scale.

The averaged trajectory was analyzed using nonlinear least-squares fitting with eq 3, and the results are summarized in Table 1.

DOI: 10.1021/acsphotonics.5b00309
ACS Photonics 2015, 2, 1451−1459

The trajectories of particles along the axis of the external electric field (x-axis) show typical step responses of underdamped systems with a natural resonant frequency ($\omega_0/2\pi$) of 225.7 Hz and β of 743.9 Hz, corresponding to a Q of approximately 1.81. The force constant and charge in Table 1 are calculated based on the TR results and assume a linear optical force as does the TR method itself. The measured force constant of 11.97 μN/m would be high for a low numerical aperture (NA) trap in a fluid, but the greater refractive index contrast between the particle and the medium generates higher trapping forces.

The transient response analysis above is only valid for linear oscillators. To verify that the optical force is linear for the excitation above we check the displacement of the particle in the constant electrostatic field after oscillations have damped to measure the DC response. Figure 4 shows the steady-state

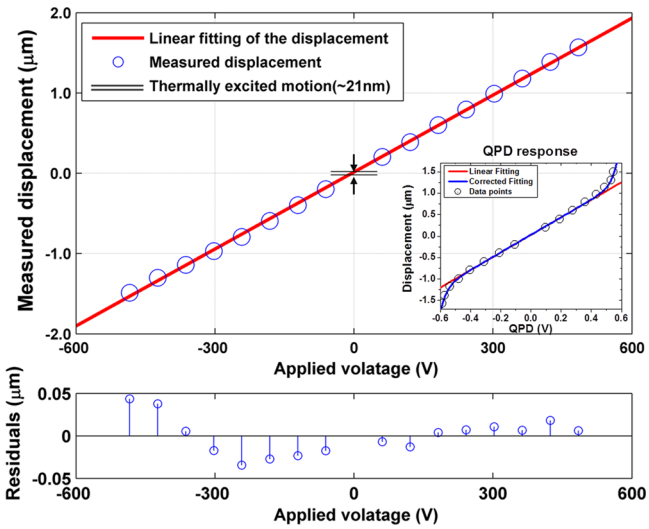

Figure 4. Linear behavior of measured displacement over a wide range as a function of applied electrostatic force ($F = qV/d$) with a fixed separation distance, d between two parallel conducting plates. Circular data points for the QPD response were measured from video microscopy using CCD trajectories under a square wave voltage applied across the parallel plates, whereas the solid red line and residual plot represent a linear fitting of the displacements and the deviation of each data point from it. The double solid line shows the limited range of motion explored by thermal fluctuations while electrostatic forcing allows us to cover a much wider range of displacement. The inset shows QPD response, which is based on the measured QPD voltage and displacement of the trapped particle. The linear QPD response was corrected to compensate the nonlinearity above 0.75 μm.

displacement values (X_0) measured as a function of applied electric field strength using the step-response. While the QPD response (Figure 4 inset) is very linear near the trap center, it departs from linearity for displacements exceeding about 1 μm, as shown in the inset. However, the video microscopy calibration described in the Methods section allows the QPD response to be corrected over the full $\pm$1.5 μm range used here. For displacements up to 0.75 μm at 300 V, the particle response is found to be very linear, which is substantially larger than the thermal displacements ($\approx$21 nm), corresponding to the range probed by the power spectral density method (double solid line in Figure 4). However, increasing the electric field magnitude much above 480 V leads to instability and jumping to a levitated trap position above the focus.

Because the transient response method used here explicitly assumes a linear harmonic oscillator, it is not directly applicable to measuring the force over a displacement range that exhibits a nonlinear response. However, direct application of Newton's equation allows arbitrary force curves to be determined by calculating the influence of the optical force on a single trajectory. Previous work in fluids has used autocorrelations to extract average velocities from Brownian motion[27,28] and measure nonconservative forces.[29] However, measurement of underdamped systems in air or vacuum with external excitation generates classical trajectories which allow direct analysis as well as measurement of a wider range of trapping forces, which should enable studies of nonlinear dynamics in optical traps.

Assuming no electrostatic field and a general optical force F_{opt} in eq 1 rather than the linear term ($\omega_0^2 = k/m$) gives,

$$x''(t) + \beta x'(t) - F_{opt}(x, t)/m = 0 \tag{4}$$

Solving for the force gives

$$F_{opt}(x) = m(a + \beta v) \tag{5}$$

where x, a and v and F_{opt} are implicitly functions of time. The velocity $v = x'(t)$ and acceleration $a = x''(t)$ are the first and second derivative of the measured displacement $x(t)$. The force as a function of displacement is given by a parametric function of time $m\{x''(t) + \beta x'(t)\}$ vs $x(t)$. For numerical differentiation (difference divided by sampling interval), we used the central difference which is the average of the forward and backward differences, $x'(t_i) \approx \{x(t_{i+1}) - x(t_{i-1})\}/2\Delta t_{sample}$. An analogous inversion without the inertial term was used by Wu et. al[29] to measure nonconservative optical forces in fluids. In contrast to the more sophisticated analysis required to extract drift velocities from random trajectories, the trajectories here trace the force curve in real-time. However, the particle mass must also be known.

An example is shown in Figure 5 (a), where measured trajectories at four different excitation voltages are plotted as parametric force (PF) curves using m and β determined by the transient response. A parametric force curve for a simulated trajectory following high voltage excitation is shown in Figure 5 (b). The vertical portions of the curves correspond to abrupt changes in apparent force as the field is turned off, with the dots along the displacement axis representing the initial positions. The ring down of the particle motion shown in Figure 3 appears here as tracing and retracing of the diagonal line (or curve for a nonlinear force). In simulated trajectories, the observed force curve is independent of excitation voltage as would be expected. Higher excitations simply measure force over larger displacements, so only one simulated force curve for 415 V excitation is shown. For measured trajectories, the force for low amplitude motion closely matches the theoretically expected behavior and is shown in red. At excitation voltages of 300 V (shown in blue), the measured force converges to the low amplitude force curve during ring down, but shows a distinctly nonlinear response immediately following excitation. Surprisingly, even though the optical force is linear with displacement at this amplitude (as shown in Figure 4), the impulse response is initially nonlinear. This behavior would not be detected using the TR method and any model that assumes a linear force would be unexpectedly misleading for cases like this. Before taking up the origin of this transitory nonlinear response we first verify the results from the PF method to establish that it agrees with the previous measurements and allows detection of general forces beyond the common assumptions of linear models or conservative forces.

DOI: 10.1021/acsphotonics.5b00309
ACS Photonics 2015, 2, 1451−1459

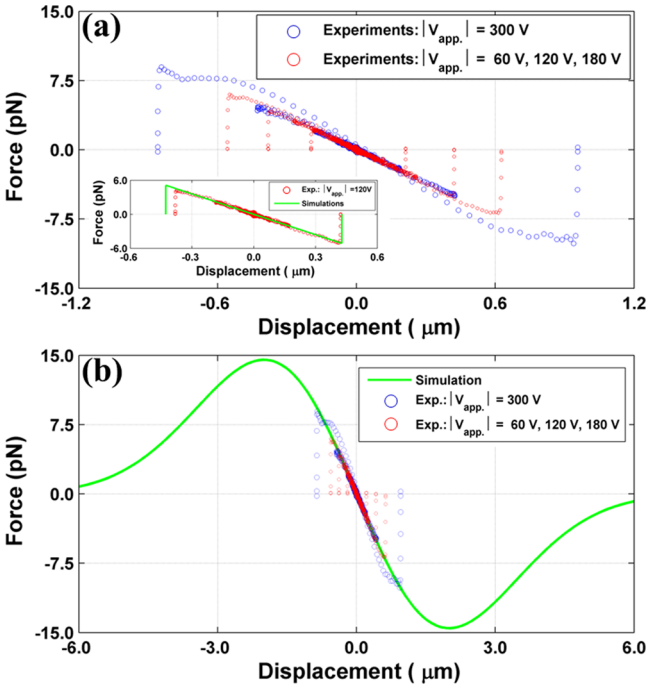

Figure 5. (a) the parametric force (PF) trajectories under various initial displacements induced by an electrostatic force. Once the particle is released from the electrostatic force, the force trajectories are measured during the entire period of damping down to the trap center. While the trajectories of the blue circles (large initial displacements) show deviations from the theoretical force curve, they eventually converge and all of the measured trajectories agree for the averaged force curve over the central region. The inset figure shows the agreement of experimental (red circular marker) and theoretical calculation results (green lines). (b) The theoretical calculation of PF trajectories demonstrates that PF can be applied over entire range of an arbitrary potential under proper forcing conditions. (Green lines are identical to green lines presented in (a) inset.)

The slope of the red PF curves at the origin gives a stiffness of (12.0 ± 0.28) μN/m, which agrees well with the previous result. (Because the focus here is on repeatability of measurements, all results are reported with purely statistical standard deviations from repeated measurement, not systematic uncertainties unless stated otherwise.) The slope is determined by a fit to the PF curve over a range ± 0.5 μm about the origin. The PF trajectory simulations numerically integrate the equation of motion of the particle in a Gaussian potential well. A Gaussian is chosen as the model potential to reproduce the observed linear behavior while testing the PF analysis of nonlinear forces at larger displacements. A half width of 2 μm is the lower bound on the well width required to reproduce the measurements. The simulated results are shown in Figure 5 (b). The simulations were performed using the experimental values of ω_0, β, and the electrostatic forcing parameters. The simulated results are analyzed identically to experimental results. The principal difference between the experimental and simulated measurements is replacing the square wave by a sawtooth wave of 415 V to stably simulate more of the force curve. This does not change the observed force curve as discussed above, and corresponds to pulling the particle to a displacement beyond 6 μm and releasing it. One parameter was not fully determined by experiment. The width of the potential can only be determined up to a lower bound, as described in the Methods section.

The simulated force curves reproduce the measurements well and also demonstrate that the PF technique is equally applicable to measuring nonlinear trapping forces. Note that the Gaussian potential used is for illustration, and recent measurements indicate that more structure in the force curve might be anticipated beyond the linear region measured here.[30,31] These simulated results do not include thermal motion which adds noise to the trajectories (as shown in Figure 5 (a)), and can lead to escape.

The simulation results demonstrate the potentially wide applicability of the parametric force (PF) method. But the deviations from the linear force curve seen in the early period of large amplitude motion highlight the limitations of 1D linear force models which are typically employed. We attribute the transitory nonlinear response observed to large amplitudes increasing departures from our initial assumptions (e.g., driving excitation of z-axis motion or varying radiometric forces). Displacement from the nominal trap axes ($y = z = 0$) before excitation would lead x excitation to generate some y and z motion. Here, the downward displacement due to gravity is roughly half the particle radius so x excitation coupling to other motion would not be surprising. Combining fast, accurate tracking in three dimensions with PF measurement should resolve the systematic differences seen for large amplitude motion resolved along only one axis and allow effectively real-time measurement of arbitrary force curves. In practice, TR can be used to measure ω_0 and β for small oscillations, and PF analysis for displacements far beyond the range of thermal excitations. The square wave excitation used here can only probe displacements less than the range corresponding to the maximum force before particles are lost, because past this point the external field will simply pull the particles from the trap. However, pulses shorter than $1/\omega_0$ or sawtooth waves can excite the particle over the full range of stably trapped trajectories. This can open a host of interesting studies of nonlinear dynamics of particle motion at high excitation, and precision 3D measurement of optical fields and forces, including comparison of the conservative and nonconservative components of optical forces.[27,29]

The technique should also be applicable to smaller particles and liquid aerosol droplets, however damping increases as radius decreases. Therefore, application to smaller particles requires higher numerical aperture beams, greater intensity, or operation in vacuum to yield under-damped systems. Nanoparticles also frequently have nonspherical shapes which complicate all optical force analysis techniques. For liquid droplets, step excitation could excite droplet vibrations. (However, the fundamental mode for a 20 μm water droplet would be above 100 kHz and the droplet shape would also be distorted by the optical trap.[32]) Maintaining sufficient induced motion by electrostatic forcing could be accomplished with a smaller gap of the parallel plates,[33,34] or more accumulation of net charge through triboelectric charging.[35] For example, our loading mechanism can increase the net charge by repeatedly contacting the particle to the glass substrate.

To validate the transient response (TR) and parametric force (PF) analysis we compared, under identical experimental conditions, measurements as performed above to the results of power spectral density (PSD) analysis and the equipartition theorem. Briefly, the trajectory following 50 pulses is measured for each run, limiting data to periods after the electrostatic field falls to zero. For TR and PF the 50 trajectories are averaged before fitting the first 15 ms of data. For the PSD the last 125 ms of each trajectory (after nearly complete damping) are used to

DOI: 10.1021/acsphotonics.5b00309
ACS Photonics 2015, 2, 1451−1459

calculate 50 PSDs which are averaged and fit. This is repeated for three voltages (60, 120, and 180 V).

The results for ω_0 and k are summarized in Table 2. The stiffness from the TR and PF methods agree very well, providing

Table 2. Trap Stiffness Results Using Three Different Methods: Power Spectrum Method Vs Transient Response and Parametric Force Analysis[a]

	power spectrum method	transient response	parametric force analysis
$\omega_o/2\pi$ [Hz]	228.14 ± 0.05	225.89 ± 1.20	
k [μN/m]	12.23 ± 0.06	11.99 ± 0.13	11.96 ± 0.20

[a]Mass =5.950 ± 0.58 pg (mean ± S.D.).

strong validation given that the TR only models a linear spring while the PF analysis makes no assumptions about the force model and fits the slope near the origin. As would be expected, the two methods do not agree as well with the PSD method to within the standard deviation of the mean. There are two reasons for this. First, the PSD method measures trap stiffness only for displacements on the order of thermal excitation (21 nm) while the TR and PF methods measure the average stiffness over a range of displacement about 50 times larger. While the optical force is still well approximated by a linear model at the level of a few percent over the range of a micrometer, the TR and PF methods are sensitive enough to resolve the fact that traps act as soft springs; i.e., the effective stiffness ultimately becomes weaker at large displacements. This stands in apparent contrast to recent observations showing traps for large particles behaving as hard springs before they soften.[30,31,36] However, differences in NA and measurement range and resolution may account for this possible discrepancy. The second potential contribution to the difference comes from the fact that the TR and PF methods average out random motion while the PSD method focuses on it. However, the PSD measurements do not distinguish thermal particle motion from other sources of apparent motion such as noise or accelerations of the lab frame. We therefore expect the TR and PF methods to give estimates of ω_0 and β that are less sensitive to noise.

This is most easily understood by comparing to the equipartition theorem. The position variance of a particle trapped in a harmonic well and in equilibrium with a fluid is[22]

$$\langle x^2 \rangle = k_B T/k \tag{6}$$

where k_B is the Boltzmann constant, T temperature in Kelvin and k is the trap stiffness. This relates the average thermal displacement to the temperature and the stiffness. But an increased variance (e.g., due to vibration or noise) corresponds to a reduced stiffness, and as the stiffness estimated by the PSD is actually larger, we attribute the difference between the PSD estimates and the transient response and parametric force estimates primarily to softening of the spring rather than noise or excess motion. At issue here is not which method provides a "better" measurement of the force curve; they measure over different ranges. Rather is it exactly what each method measures and how to combine them to yield the most complete picture of the process components and interactions: particle, medium, and optical beam.

Finally, we can use equipartition to assess whether the fluctuations we observe are consistent with Brownian motion and to what extent experimental noise or vibration contribute. We must first determine whether the particle is heated by the laser beam, as both temperature and experimental noise give rise to measured fluctuations. To estimate the temperature from the damping we can use the Stokes equation.[20] This entails no additional assumptions, just viscous damping for a spherical particle. The TR measurement of β is well suited to this because it rejects noise. The β measured by the TR (742 ± 25 Hz) is higher than the value expected from Stokes law for a fluid at 20 °C (640 Hz, neglecting the slip correction factor,[37] which is only on the order of 0.76%). If we attribute the increase in damping over the expected value to increased temperature, we can estimate the temperature to be 80 °C using Stokes law and Sutherland's values[38] for the viscosity of air as a function of temperature.

Our TR measurements of a stiffness of 11.90 μN/m at the estimated temperature of 80 °C correspond to a thermal displacement standard deviation of 20.27 nm while our measured value is slightly higher at 21.00 nm, indicating that the measured displacement fluctuations are dominated by thermal noise rather than convection or technical noise.

To summarize the calculations used here, we extract the natural resonant frequency (ω_0), damping (using β, ς, or Q as the measure), and displacement (X_0) under a constant field from the fit of the transient response to eq 3. Using the diameter (D) measured from image analysis and the material density (ρ_{PS}) given by the manufacturer, we calculate the particle mass ($m = \rho_{PS}4/3\pi(D/2)^3$), which is gives the trap stiffness ($k = m\omega_0^2$). The induced displacement (X_0) under a uniform electric field ($E = V/d$) is used to calculate the net charge ($q = kX_0d/V$). The mass and damping then allow the full nonlinear parametric force to be calculated from the trajectory. Finally, Stokes law and Sutherland's formula for the viscosity of air allows the air temperature to be calculated that would give the measured damping. Equipartition ($\langle x^2 \rangle = k_B T/k$) is then used to estimate the position variance from T and k. The values of ω_0, β, and D are measured directly, while the values of m, k, q, F_{opt}, and T depend on ρ_{PS}.

We have demonstrated a new method (parametric force analysis) based on electrostatic forcing to measure optical forces on trapped particles simply and precisely. Simulations demonstrate that it should be equally applicable to nonlinear forces and regions well beyond the nominal trapping volume assuming only that the behavior is modeled by Newton's equations with viscous damping. Laboratory measurements show departures from the simple one-dimensional model that demonstrates the ability to resolve nonlinear behavior under impulse excitation. Comparisons to measurements for small displacements based on the transient response and power spectral density methods give good agreement and allow the temperature and the excess variance to be estimated. In all, assuming only the manufacturer's value for the density of the particle, we are able to determine values for the particle size, mass, charge, temperature, the damping, and viscosity of the air, as well as the stiffness and, in principle, the full force curve of the trap.

METHODS

Experimental Setup. The optical tweezers setup was developed using a commercial inverted optical microscope (Eclipse TE2000, Nikon Instruments Inc.) installed on an optical table with a passive vibration isolation system. A diode pumped neodymium yttrium vanadate (Nd:YVO_4) laser with maximum optical power of 5 W at a wavelength of 1064 nm (J20I-8S-12K/BL-106C, Spectra Physics) was used for trapping. The incident optical power was chosen (or modulated) by changing the bias voltage of an electro-optic modulator (EOM) (350−80LA/Driver 302RM, Con-Optics Inc.). To provide a well-polarized

DOI: 10.1021/acsphotonics.5b00309
ACS Photonics 2015, 2, 1451−1459

TEM_{00} beam with optimal trapping efficiency, the beam was delivered through a polarization-maintaining single mode optical fiber (P1−1064PM-FC-5, THORLABS Inc.) and collimated by a fiber collimator (F810FC-1064, THORLABS Inc.). The beam diameter out of the collimator (8 mm) slightly under-filled (filling ratio = 0.8, defined as the ratio of the laser beam diameter to the objective back aperture diameter) the back aperture of a near-infrared (NIR) corrected long-working distance (LWD) objective lens (Mitutoyo, 20×, NA = 0.4, WD = 20 mm).[39] Once the particle is trapped, its motion is measured using a quadrant-cell photodetector (QPD), which is calibrated using a charge-coupled device (CCD) camera. Briefly, the transmitted IR light is collected by a condenser lens (aspheric lens, WD = 16 mm and NA = 0.26) and projected onto the center of the QPD (QPD-2031, Newport), which measures the movement of the focused spot induced by the particle's motion. An additional lens and mirror was placed between the condenser lens and QPD to direct and conjugate the back focal plane of the condenser and the center of QPD. For the reflected light imaging, a halogen lamp (HAL100, Nikon) was coupled into the objective lens and captured using a CCD camera (Flea3, Point Grey) with a dichroic mirror to filter out the IR light. Additionally, to retain a complete three-dimensional view, the particle can also be imaged horizontally using an aspherized achromatic lens (with an effective focal length of 14 mm) with bright field illumination from a fiber-coupled white light LED.

QPD Calibration. The QPD is calibrated in two steps to map the measured QPD voltage signals onto physical trajectories (particle position in μm as a function of time). First, the overall CCD magnification is calibrated using a Ronchi ruling, which allows both diameter and transverse (x, y) displacement of levitated particles to be measured. A reflected image of a Ronchi grating with 100 lines per mm (Model: 38562, Edmunds Optics) is captured using the LWD objective (20×, NA = 0.4) and CCD (Flea3, Point Grey) camera attached to the optical microscope. The reflected image profiles of the grating are averaged along the line of grating, and the average pixel pitch is found to be 0.158 μm. Then the motion of a slowly oscillating trapped particle is measured simultaneously in the CCD and QPD to calibrate the QPD response. The CCD images are analyzed using the particle tracking tool of ImageJ to extract particle position measurements.[40]

For a given step voltage, the average positions of the particle before the step and after ring down are taken as reference positions, and the displacement between them is measured using the CCD (in μm using the previous calibration) and the QPD (in volts). This effectively measures the displacement of a particle from trap center (field-free position) as a function of a static DC voltage as well as any nonlinearity in the QPD response. This calibration is repeated for every trapped particle and we define the QPD detection sensitivity α as the ratio of particle displacement to QPD voltage $x_{\mathrm{length}}(t) = \alpha \mathrm{V}(t)$. Here we restrict particle motion to the linear range of QPD response, which generates displacements less than 10% of the particle radius. From the image sequences of a representative trapped particle captured at 60 frames per second with 2 Hz of square wave excitation, the averaged QPD detection sensitivity was found to be $\alpha = (2.043 \pm 0.03)\ \mu\mathrm{m\ V}^{-1}$.

Particle Size Determination. Dry powders of polystyrene (PS) particles were used (Dri-CalTM size standards DC-20, diameter = 20.0 μm ± 0.9 μm, Thermo Scientific). Solid PS 20 μm particles are used to reduce size variance with better sphericity. The particle size was measured by digital microscopy of the trapped particle using the CCD shown in Figure 1. First the CCD is calibrated using the Ronchi ruling as described for displacement measurement. Then the image is thresholded to determine the sphere diameter and the circular area calculated using the ImageJ software package. The threshold is varied and the average diameter from nine measurements using different values of the threshold is used to minimize potential artifacts from the selection of threshold values. Mie scattering can be used where more accurate measurement of dimension and shape is required, potentially including in situ measurement of refractive index and other particle properties.[41] The diameter of the particle used for our experiment was 22.12 μm ± 0.58 μm, with the mass calculated using the particle density provided by the manufacturer ($\rho_{\mathrm{PS}} = 1.05\ \mathrm{g/cm^3}$). The ±0.58 μm spread reported for the particle size results from different focal positions yielding slightly different values.

Sample Preparation and Loading. The charge of our particles is typically a few thousand electrons and depends on the preparation method, contact with the substrate, and the duration of exposure to air in the lab. Under an electrostatic field imposed by applying a voltage V across the two ITO-coated coverslips (separated by a distance d), the force on the particle will be $F = qV/d$, where q is the total charge (approximately 3990 electrons for the measurements reported here). The variation in the magnitude of the electric field due to fringe fields is estimated to be less than 1% for particle positions within 1 mm of the center.

To minimize agglomeration of the particles, just before use small amounts of particles were taken from the container with a 1 mm diameter glass capillary tube and then spread out over a glass coverslip with a gentle tap. The coverslip is attached to a ring-type PZT installed between the objective lens and focal plane to detach the target particle using resonant driving of the PZT (American Piezo Company).[21] To launch and trap a particle, a selected particle on the coverslip is moved into the trapping beam and launched by triggering a pulse at the resonant frequency of the PZT assembly. This momentarily breaks the adhesion between the particle and substrate, so that the radiation pressure of trapping laser lifts the particle into the trapping volume while the CCD images the process in real time. Once the particle is trapped, it is moved about 10 mm above the surface of substrate using the motorized focusing stage (MFS) so that no other objects or surfaces hydrodynamically affect the motion of the trapped particle.[42] After the particle is successfully transferred, it has never been observed to fall from the trap unless it exposed to external forces such as external air flow.

Sample Enclosure and Electrostatic Forcing. To protect the trapped particle from external air flow, a rectangular glass enclosure (width × height × separation: 18 mm × 10 mm × 15 mm) was fabricated with glass coverslips held in a frame. The frame was made from biodegradable thermoplastic polylactide (PLA) using three-dimensional printing. Each of the five windows (the bottom side is directly attached to the PZT) are covered with transparent thin cover glasses and sealed with silicone rubber. Among the four side-windows of the enclosure, one pair of two side windows facing each other are made from indium tin oxide (ITO) coated cover glass (0.7 mm thick, 18 mm × 18 mm, resistivity of 50 Ω per square) to enable electrostatic forcing across the two plates without losing optical accessibility. Thus, we are able to measure the motion of a trapped particle in air under external electrostatic-fields modulated using a waveform generator (HP33250A, Agilent: rise/fall time <8 ns) connected to a high-voltage power amplifier (PZD700A M/S, TREK Inc.) with a slew

DOI: 10.1021/acsphotonics.5b00309
ACS Photonics 2015, 2, 1451−1459

rate of 380 V/μs and output voltage up to ±700 V over the signal bandwidth from DC to 150 kHz (−3 dB).

Temperature and Damping. We assume the temperature of the particle and the air to be approximately the same. The mean free path is less than 1/100 of the particle diameter so we estimate heating for the hydrodynamic case. Solving the heat equation for a spherical particle in a stagnant fluid shows the air temperature within the range of displacement to remain constant to within a few percent, and the time scale for equilibration to be fast compared to our sampling time. This neglects convection, however. Particle motion drives air flow over the surface so precision measurements of particle motion may reveal interesting aspects of the heat transport and associated behavior.

Radiometric Forces. Since the trapped particle is continuously influenced by air currents and molecular collisions, the motion of the trapped particle can include Brownian motion and pressure driven flow. The ensemble averaging used here reduces the measured Brownian motion and motion due to random flow. It is not expected to reduce radiometric forces or the effects of systematic flows, such as convection due to nonuniform heating of the cell or air by the laser. The most prominent radiometric force would be expected to operate perpendicular to our axis of measurement. However, particle motion along the x axis will deflect the optical beam, potentially giving rise to temperature gradients in the particle parallel to the x axis. A sustained radiometric force would be included in the force measured here if it were stable in time, a function of position, and generated a force along the x axis (perhaps via z-axis motion in the optical potential). Otherwise radiometric effects would be averaged over. Furthermore, these forces would be reduced by performing the experiment in vacuum.

Simulation Details. To simulate trajectories, Newton's equation is integrated for an initial position and velocity of zero. An inhomogeneous term represents the pulsed field: $x''(t) + \beta x'(t) + \omega_0^2 x(t) e^{-x^2(t)/2\sigma^2} = A_{\mathrm{elec}} S(t)$, where A_{elec} is the electrostatic acceleration ($A_{\mathrm{elec}} = 415\ \mathrm{V} \times qe/dm$), and $S(t)$ is a 2 Hz sawtooth wave with 50% duty cycle that linearly rises to one then drops to zero. In the above, e is charge of the electron, σ is the potential width, and all other variables are as previously defined. All parameters in the equation are measured in the lab (Table 1 and 2) except the potential width sigma σ. Only the lower bound on sigma may be estimated since the stiffness alone is not adequate to calculate both the depth and width of a Gaussian potential. There are no other free or fit parameters. The equation is solved numerically using the NDSolve routine in Mathematica with an implicit backward differentiation method.

AUTHOR INFORMATION

Corresponding Author

*E-mail: lebrun@nist.gov.

Notes

The authors declare no competing financial interest.

ACKNOWLEDGMENTS

All work performed under the support of the National Institute of Standards and Technology.

REFERENCES

(1) Chavez, I.; Huang, R.; Henderson, K.; Florin, E.-L.; Raizen, M. G. Development of a Fast Position-Sensitive Laser Beam Detector. *Rev. Sci. Instrum.* **2008**, *79*, 105104.

(2) Gittes, F.; Schmidt, C. F. Interference Model for Back-Focal-Plane Displacement Detection in Optical Tweezers. *Opt. Lett.* **1998**, *23*, 7−9.

(3) Li, T.; Kheifets, S.; Medellin, D.; Raizen, M. G. Measurement of the Instantaneous Velocity of a Brownian Particle. *Science* **2010**, *328*, 1673−1675.

(4) Neuman, K. C.; Nagy, A. Single-Molecule Force Spectroscopy: Optical Tweezers, Magnetic Tweezers and Atomic Force Microscopy. *Nat. Methods* **2008**, *5*, 491−505.

(5) Phillips, W. D. Nobel Lecture: Laser Cooling and Trapping of Neutral Atoms. *Rev. Mod. Phys.* **1998**, *70*, 721−741.

(6) Visscher, K.; Gross, S. P.; Block, S. M. Construction of Multiple-Beam Optical Traps with Nanometer-Resolution Position Sensing. *IEEE J. Sel. Top. Quantum Electron.* **1996**, *2*, 1066−1076.

(7) Neuman, K. C.; Block, S. M. Optical Trapping. *Rev. Sci. Instrum.* **2004**, *75*, 2787−2809.

(8) Moffitt, J. R.; Chemla, Y. R.; Smith, S. B.; Bustamante, C. Recent Advances in Optical Tweezers. *Annu. Rev. Biochem.* **2008**, *77*, 205−228.

(9) Li, T.; Kheifets, S.; Raizen, M. G. Millikelvin Cooling of an Optically Trapped Microsphere in Vacuum. *Nat. Phys.* **2011**, *7*, 527−530.

(10) Maragò, O. M.; Jones, P. H.; Gucciardi, P. G.; Volpe, G.; Ferrari, A. C. Optical Trapping and Manipulation of Nanostructures. *Nat. Nanotechnol.* **2013**, *8*, 807−819.

(11) Gieseler, J.; Deutsch, B.; Quidant, R.; Novotny, L. Subkelvin Parametric Feedback Cooling of a Laser-Trapped Nanoparticle. *Phys. Rev. Lett.* **2012**, *109*, 103603.

(12) Burnham, D. R.; Reece, P. J.; McGloin, D. Parameter Exploration of Optically Trapped Liquid Aerosols. *Phys. Rev. E* **2010**, *82*, 051123.

(13) Summers, M. D.; Burnham, D. R.; McGloin, D. Trapping Solid Aerosols with Optical Tweezers: A Comparison between Gas and Liquid Phase Optical Traps. *Opt. Express* **2008**, *16*, 7739−7747.

(14) Knox, K. J.; Burnham, D. R.; McCann, L. I.; Murphy, S. L.; McGloin, D.; Reid, J. P. Observation of Bistability of Trapping Position in Aerosol Optical Tweezers. *J. Opt. Soc. Am. B* **2010**, *27*, 582.

(15) Millen, J.; Deesuwan, T.; Barker, P.; Anders, J. Nanoscale Temperature Measurements Using Non-Equilibrium Brownian Dynamics of a Levitated Nanosphere. *Nat. Nanotechnol.* **2014**, *9*, 425−429.

(16) Gieseler, J.; Novotny, L.; Quidant, R. Thermal Nonlinearities in a Nanomechanical Oscillator. *Nat. Phys.* **2013**, *9*, 806−810.

(17) Le Gall, A.; Perronet, K.; Dulin, D.; Villing, A.; Bouyer, P.; Visscher, K.; Westbrook, N. Simultaneous Calibration of Optical Tweezers Spring Constant and Position Detector Response. *Opt. Express* **2010**, *18*, 26469−26474.

(18) Tolić-Nørrelykke, S. F.; Schäffer, E.; Howard, J.; Pavone, F. S.; Jülicher, F.; Flyvbjerg, H. Calibration of Optical Tweezers with Positional Detection in the Back Focal Plane. *Rev. Sci. Instrum.* **2006**, *77*, 103101.

(19) Allersma, M. W.; Gittes, F.; DeCastro, M. J.; Stewart, R. J.; Schmidt, C. F. Two-Dimensional Tracking of ncd Motility by Back Focal Plane Interferometry. *Biophys. J.* **1998**, *74*, 1074−1085.

(20) Bykov, D. S.; Schmidt, O. A.; Euser, T. G.; Russell, P. S. J. Flying Particle Sensors in Hollow-Core Photonic Crystal Fibre. *Nat. Photonics* **2015**, *9*, 461−465.

(21) Ashkin, A.; Dziedzic, J. M. Optical Levitation by Radiation Pressure. *Appl. Phys. Lett.* **1971**, *19*, 283−285.

(22) Chandrasekhar, S. Stochastic Problems in Physics and Astronomy. *Rev. Mod. Phys.* **1943**, *15*, 1−89.

(23) Collin, D.; Ritort, F.; Jarzynski, C.; Smith, S. B.; Tinoco, I.; Bustamante, C. Verification of the Crooks Fluctuation Theorem and Recovery of RNA Folding Free Energies. *Nature* **2005**, *437*, 231−234.

(24) Florin, E.-L.; Pralle, A.; Stelzer, E. H. K.; Hörber, J. K. H. Photonic Force Microscope Calibration by Thermal Noise Analysis. *Appl. Phys. A: Mater. Sci. Process.* **1998**, *66*, S75−S78.

(25) Simmons, R. M.; Finer, J. T.; Chu, S.; Spudich, J. A. Quantitative Measurements of Force and Displacement Using an Optical Trap. *Biophys. J.* **1996**, *70*, 1813−1822.

(26) Thornton, S. T.; Marion, J. B. *Classical Dynamics of Particles and Systems*, 5th ed.; Brooks/Cole: Pacific Grove, CA, 2003.

(27) Roichman, Y.; Sun, B.; Stolarski, A.; Grier, D. G. Influence of Nonconservative Optical Forces on the Dynamics of Optically Trapped

DOI: 10.1021/acsphotonics.5b00309
ACS Photonics 2015, 2, 1451−1459

Colloidal Spheres: The Fountain of Probability. *Phys. Rev. Lett.* **2008**, *101*, 128301.
(28) Pesce, G.; Rusciano, G.; Zito, G.; Sasso, A. Simultaneous Measurements of Electrophoretic and Dielectrophoretic Forces Using Optical Tweezers. *Opt. Express* **2015**, *23*, 9363−9368.
(29) Wu, P.; Huang, R.; Tischer, C.; Jonas, A.; Florin, E.-L. Direct Measurement of the Nonconservative Force Field Generated by Optical Tweezers. *Phys. Rev. Lett.* **2009**, *103*, 108101.
(30) Richardson, A. C.; Reihani, S. N. S.; Oddershede, L. B. Non-Harmonic Potential of a Single Beam Optical Trap. *Opt. Express* **2008**, *16*, 15709.
(31) Godazgar, T.; Shokri, R.; Reihani, S. N. S. Potential Mapping of Optical Tweezers. *Opt. Lett.* **2011**, *36*, 3284−3286.
(32) Hill, R. J. A.; Eaves, L. Vibrations of a Diamagnetically Levitated Water Droplet. *Phys. Rev. E* **2010**, *81*, 056312.
(33) Moore, D. C.; Rider, A. D.; Gratta, G. Search for Millicharged Particles Using Optically Levitated Microspheres. *Phys. Rev. Lett.* **2014**, *113*, 251801.
(34) Beunis, F.; Strubbe, F.; Neyts, K.; Petrov, D. Beyond Millikan: The Dynamics of Charging Events on Individual Colloidal Particles. *Phys. Rev. Lett.* **2012**, *108*, 016101.
(35) Soh, S.; Liu, H.; Cademartiri, R.; Yoon, H. J.; Whitesides, G. M. Charging of Multiple Interacting Particles by Contact Electrification. *J. Am. Chem. Soc.* **2014**, *136*, 13348−13354.
(36) Jahnel, M.; Behrndt, M.; Jannasch, A.; Schäffer, E.; Grill, S. W. Measuring the Complete Force Field of an Optical Trap. *Opt. Lett.* **2011**, *36*, 1260−1262.
(37) Cunningham, E. On the Velocity of Steady Fall of Spherical Particles through Fluid Medium. *Proc. R. Soc. London, Ser. A* **1910**, *83*, 357−365.
(38) Smits, A. J.; Dussauge, J.-P. *Turbulent Shear Layers in Supersonic Flow*; Springer: Berlin, 2006.
(39) Mahamdeh, M.; Campos, C. P.; Schäffer, E. Under-Filling Trapping Objectives Optimizes the Use of the Available Laser Power in Optical Tweezers. *Opt. Express* **2011**, *19*, 11759−11768.
(40) Sbalzarini, I. F.; Koumoutsakos, P. Feature Point Tracking and Trajectory Analysis for Video Imaging in Cell Biology. *J. Struct. Biol.* **2005**, *151*, 182−195.
(41) Chylek, P.; Ramaswamy, V.; Ashkin, A.; Dziedzic, J. M. Simultaneous Determination of Refractive Index and Size of Spherical Dielectric Particles from Light Scattering Data. *Appl. Opt.* **1983**, *22*, 2302.
(42) Burnham, D. R.; McGloin, D. Radius Measurements of Optically Trapped Aerosols through Brownian Motion. *New J. Phys.* **2009**, *11*, 063022.

DOI: 10.1021/acsphotonics.5b00309
ACS Photonics 2015, 2, 1451−1459